Numerical and experimental study on the Duisburg Propeller Test Case

Chiara Wielgosz[*,†], **Rafael Golf**[*], **Artur K. Lidtke**[‡], **Guilherme Vaz**[*,‡,§] **and Ould el Moctar**[*]
[*]ISMT, University of Duisburg-Essen, Duisburg/Germany, [†]MARIN Academy, Wageningen/The Netherlands, ‡MARIN, Wageningen/The Netherlands, §WavEC-Offshore Renewables, Lisbon/Portugal
chiara.wielgosz@uni-due.de

1 Introduction

Understanding of cavitation behaviour on marine propellers is of critical importance to ship designers as it dictates several of the operating limits of the propulsor due to onset of increased erosion risk or unacceptable levels of noise and vibration. Consequently, this topic continues to inspire experimental studies aimed at providing a more in-depth understanding of the physical phenomena involved, but also to provide means of validation for numerical models. Unfortunately, many of these studies do not cover the complete spectrum of types of cavitating flows seen in practice on modern ship propellers and do not present uncertainties of the experimental data. Present work aims to address these issues by reporting on a new series of quantitative and qualitative model-scale propeller tests on the Duisburg Propeller Test Case (DPTC). The experimental data is then used to validate Computational Fluid Dynamics (CFD) predictions of open water performance and cavitation patterns and a verification and validation study is carried out.

2 Experimental methodology

The experiments were carried out at the Institute of Marine Technology, Maritime Engineering and Transport Systems (ISMT) in the 'Kavitationstunnel K23'.The tunnel working section has a cross section of 0.3 m x 0.3 m. The propeller is connected to a J19 Kempf & Remmers dynamometer mounted at the end of the rotating shaft. This measuring unit is capable of recording thrust, torque and rotational speed of the propeller; to measure the pressure inside the tunnel, a pressure sensor, positioned at the upstream end of the test section, was used. Velocities were calculated from the recorded value of pressure difference between two sections upstream of the working section. The propeller is the P1570 model of SVA (Report 3733), designed to be representative of those used on contemporary vessels, which was also used on the container ship of the Duisburg Test Case project, el Moctar et al. (2012). The general characteristics and schematic representation of the propeller can be found in Figure 1 and Table 1. Additional details about the experimental study are reported by Golf (2018).

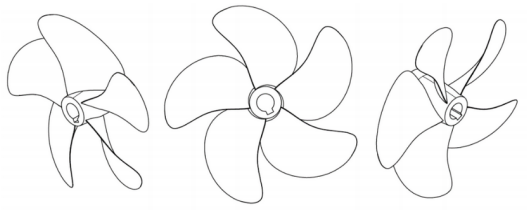

Fig. 1: Schematic representation of the P1570 SVA propeller (Report 3733), (Golf , 2018)

Table 1: Characteristics of the SVA P1570 propeller (Report 3733).

Parameter	Value	Unit
Diameter	0.150	[m]
Chord length at r/R=0.7	0.054	[m]
Effective skew angle	31.970	[deg]
Pitch/Diameter ratio at r/R=0.7	0.800	[-]
Effective area/Disk area ratio	0.800	[-]

2.1 Open water tests

The model was tested in open water inside the cavitation tunnel in wetted conditions over a range of advance coefficients $J = V_A/nD$ (where V_A is the inlet speed, n the propeller rotation rate, and D its diameter) and the open water characteristics were recorded for five different rotational speeds: 720, 1080, 1500, 2000 and 2500 RPM, with corresponding inlet velocities adjusted to maintain a constant advance ratio J range. The highest Reynolds number value for 2000 RPM at the tip of the blades is $Re(R) = 8.18 \cdot 10^5$ (where $Re(R) = R \cdot v_{ref}/\nu$ being R the propeller's radius, $v_{ref} = \sqrt{({V_A}^2 + (2\pi n 0.7R)^2)}$ the relative velocity and ν the kinematic viscosity of water) showing that the flow has a transitional nature. Tests without the propeller installed on the shaft were run for the highest inlet velocity of each

measurement series to record thrust and torque corrections. For what concerns the calculation of the uncertainties, measurements for inlet velocity, rotational speed, thrust T and torque Q were logged every 10 seconds over a 1 minute span for three velocities (low, medium, high) of the open water diagram. Following the measurements, the average of the standard deviation was computed and the uncertainties were assessed through the 'Gaussian error propagation law' (Dinter , 2011) to obtain uncertainties for the thrust coefficient $K_T = T/\rho n^2 D^4$ (with ρ density of water), the torque coefficient $10K_Q = 10Q/\rho n^2 D^5$, the open water efficiency $\eta_O = JK_T/2\pi K_Q$ and the advance ratio J, rare values found in experimental studies. It was observed that lower rotational speed tests were less credible due to the high impact of the velocity uncertainty on the actual measured values of interest.

2.2 Cavitation tests

A systematic cavitation inception study was performed by varying the inlet velocity and the static pressure p_∞ to determine the operational regions where the different cavitation topology could be observed. The rotational speed was kept constant at 2000 RPM. The cavitation structures that have been observed were: hub vortex, single bubble, tip vortex, sheet cavitation, cloud cavitation, pressure side cavitation and supercavitation. In addition, at the advance ratio $J = 0.60$, a study on the reduction of thrust and torque due to the presence of cavitation was carried out. In this case, measurements without the propeller installed on the shaft reported thrust corrections for each pressure step but no torque corrections.

3 Numerical methodology

Simulations were performed using the Computational Fluid Dynamics code ReFRESCO version 2.5.0 (www.refresco.org), developed by MARIN in collaboration with several universities. The code is based on the finite volume, face-based approach, with the flow variables collocated at the cell centers and the equations coupled via a segregated SIMPLE-type algorithm. The wetted and cavitating flow conditions were simulated by solving the RANS equations with the $k - \sqrt{k}L$ model for turbulence by Menter et al. (2006). This has been reported to produce less eddy viscosity than the more commonly used $k - \omega$ SST model, for instance, providing improved convergence (Rijpkema et al. (2015)) and better modelling of cavitation dynamics. Eddy viscosity and turbulence intensity were set at the inlet to reproduce a turbulence intensity of 3%, as observed during the experiments. The convective fluxes were discretised using the second order LIMITED QUICK scheme for the momentum equations and a first order upwind scheme for the turbulence equation. To compute the open water wetted flow propeller performance, steady simulations were performed by using the Absolute Frame of Motion (AFM) approach, where the governing equations are solved with respect to the body-fixed reference system and the flow variables are expressed with respect to the earth-fixed reference system. Cavitation was modelled using a homogeneous mixture-based approach, the source term in the transport equation was based on Sauer and Schnerr (2001) model chosen due to the more realistic results as seen in Vaz et al. (2015), and the equation was discretized with a first order upwind scheme. The cavitating flow simulations were unsteady and the temporal discretisation was obtained by applying a second order implicit three-time-level scheme. Data of the water temperature during the experiments were not methodically registered and standard water properties, computed based on the average temperature recorded during the tests, were used in the simulations.

The numerical domain consisted of two cylindrical sub-domains: an 'internal' one containing the rotating propeller and hub, and an 'external' one representing the cavitation tunnel and containing the non-rotating part of the shaft. The stator domain extended 5 propeller diameters upstream and 10 downstream to reproduce the open water condition avoiding effects of the boundaries, and had a radius of 1.13 diameter to achieve a cross-section area equivalent to the one of the cavitation tunnel in order for the blockage effects present in the experiments to be accounted for. Fixed velocity and turbulent quantities were prescribed at the inlet, while fixed pressure was specified on the part of the outlet extending outside of the propeller slipstream. An outflow boundary condition was used in the middle of the outlet to reduce the effect of boundaries on the jet of the accelerated fluid created by the propeller. The propeller, the hub and the shaft were specified as no-slip walls, the outer wall of the stator as slip-walls and the interfaces between the two sub-domains were treated as sliding interface boundaries with a first order

nearest-cell interpolation method. Six different geometrically similar grids were designed for the rotor using a structured grid generator, while two grids, corresponding to the coarsest and a medium cell densities, were generated for the stator. This decision was taken to allow a higher cell density in the rotor, prioritising the region close to the propeller where more challenging flow phenomena were expected, while saving computational time with a coarser grid for the stator, where the flow is of less interest. The stator grids included 1.1 and 10.6 million cells, while the propeller domains contained between 2.9 and 40.7 million cells. Maximum y^+ of 0.533 was found on the coarsest grid in open water conditions for advance ratio of 0.80.

3.1 Open water simulations

A verification and validation study was carried out for the rotational speed of 2000 RPM. The methodology based on Eça and Hoekstra (2014) was applied, assuming that the leading numerical error was the discretization error and that iterative and round-off errors were negligible in comparison. Round-off errors can be considered negligible since double precision was used, as well as the iterative error since L_{inf} norm residuals were two order of magnitude smaller than the discretization error (Eça and Hoekstra , 2009). After this study, carried out for design J value of 0.80, a grid of medium cell density with a total of 23.8M cells (grid $f0.550$) was chosen to simulate the experimental conditions due to a good compromise between number of cells and quality of the results. Values for L_{inf} norm residuals were required to be lower than 10^{-6} for the convergence to be considered acceptable; when this condition could not be met, due to the presence of flow separation or high loading, a minimum criterion of L_2 norm residuals being two orders of magnitude less than L_{inf} norm residuals was used, with values for L_2 norm residuals not higher than 10^{-5} and checking the location of the cells with the highest residuals.
The validation procedure suggested in ASME (2009) was used to address modeling errors of the thrust coefficient K_T, the torque coefficient $10K_Q$ and the open water efficiency η_O, adopting a 'strong-model' and expanded uncertainties U_{95} with a coverage factor $k = 2$ due to the derivation of the experimental uncertainties u_D from the standard deviation. Three different numerical uncertainties u_{num} (Eça and Hoekstra (2014)) were computed as a function of the flow topology; for the interval of advance ratio $0.28 \leq J \leq 0.68$ the limiting streamlines show separation of the flow and the numerical uncertainties were estimated over the four coarsest grids for a value of advance ratio $J = 0.44$. For the interval $0.72 \leq J \leq 0.92$ separation is not present and the numerical uncertainties obtained for $J = 0.80$ were used. An additional numerical uncertainty is computed for the higher advance coefficient values $0.96 \leq J \leq 1.02$ due to the vicinity to the zero-thrust condition. Numerical uncertainty for this regime was estimated at the advance ratio value of 0.98 using the four coarsest grids.

3.2 Cavitation simulations

Two different operating points were selected for simulating cavitation behaviour. These were differentiated by different cavitation numbers $\sigma_{0.7} = (p_\infty - p_v)/0.5\rho(V_A^2 + (\pi n 0.7D)^2)$ (where p_v is the vapour pressure) and advance coefficients J. These two specific points were chosen due to the evident presence of sheet cavitation (Point 1 with $\sigma_{0.7} = 0.227$ and $J = 0.596$) and tip vortex cavitation (Point 2 with $\sigma_{0.7} = 0.396$ and $J = 0.60$). Simulations were carried out using the medium density grid $f0.550$ and the cavity extent was compared with the available experimental photographs from the experiments. The adopted time step was equal to 0.25° of propeller rotation (Vaz et al. , 2015) and the flow was simulated for five propeller rotations for Point 1 and eight propeller rotations for Point 2 to achieve values for L_2 norm residuals lower than 10^{-4} and L_{inf} norm residuals lower than 10^{-2} for all flow quantities. Higher residual values were accepted due to the more complicated physics present in these simulations.

4 Results

4.1 Open water performance

Comparison between experimental and numerical results for the open water diagram obtained for a propeller rotation rate of 2000 RPM is depicted in Figures 2 and 3, where the percentage difference was calculated applying the formula $\%\ difference = (\phi_{num} - \phi_{exp}) * 100/(\phi_{exp})$ and for clarity values of advance ratios J close to zero-thrust condition were omitted. The comparison shows that, for the interval

of advance ratios J from 0.68 to 0.88 the numerical difference between the two solutions is within 4% of the measured value; for the lower J where higher loading and a leading edge vortex are present, the comparison is worse with the numerical solution over-estimating propeller forces and moments by up to 8% of the experimentally reported value. At advance coefficients above 0.9, the propeller approaches the zero-thrust condition, making a quantitative comparison with the experiments less meaningful. Nevertheless, the overall trend in variation of K_T, $10K_Q$ and η_O is well represented. By interpolating experimental and numerical data to find the value of the advance coefficient J for which the zero-thrust condition is obtained, an acceptable agreement was found, with an experimental advance ratio J equal to 1.015 and the numerical value equal to 1.014. The above comparison does not take into account experimental u_D and numerical u_{num} uncertainties. The verification study asserts that the highest numerical uncertainties are present for the highest range of advance ratios ($0.96 < J < 1.02$), with $u_{num}(K_T) = 1.1\%$, $u_{num}(10K_Q) = 2.9\%$ and $u_{num}(\eta_O) = 2.1\%$ as visible in Table 2. In the case of experimental uncertainties, the highest values for the advance ratio uncertainties were found for 720 RPM with values up to 10%, decreasing with increasing rotational speed to a value of 4% for rotational speed of 2500 RPM. Similar behavior was found for all the other experimental uncertainties, thrust coefficient uncertainties varied from 9% to 1%; for the torque coefficient uncertainty values varied from 3% to 0.4% and for open water efficiency from 8% down to 5%. The validation analysis shows that each studied variable behaves differently; for the thrust coefficient the estimated uncertainty intervals contain values of the modeling error equal to zero from $J = 0.68$ forward, with an over-estimation of the average between experimental and numerical K_T up to 12% and an under-estimation up to 11% (Figure 4a). For the torque coefficient $10K_Q$ (Figure 4b), an over-estimation of the averaged $10K_Q$ up to 9% and an under-estimation up to 9% are visible. In Figure 4c corresponding to the open water efficiency, it is possible to observe that all the derived model uncertainty intervals contain the model error zero-value, with an over-estimation of the efficiency over 13% and an under-estimation up to 8%. For all three variables, the model uncertainties are caused by both experimental and numerical uncertainties roughly of the same magnitude, as visible in Figure 2 where none of the error bars is visibly dominating. Comparison error values are high, compared to previous studies (Vaz et al. , 2015), because of the transitional nature of the flow ($Re(R) = 8.18 \cdot 10^5$) and of systematic errors in the experiments (thrust correction measured solely for the highest inlet speeds). The values of advance ratios close to zero-thrust condition were omitted in Figure 4 for clarity.

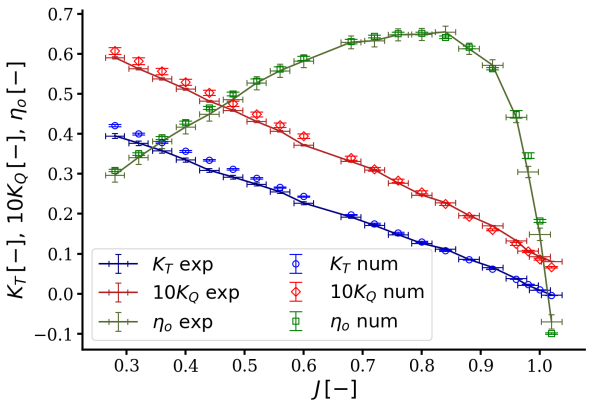

Fig. 2: Comparison between experimental results and uncertainties, Golf (2018), and numerical results and uncertainties of the open water diagram for 2000 RPM.

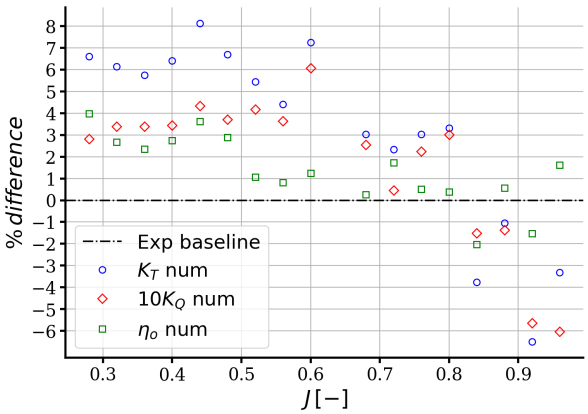

Fig. 3: Percentage difference between experimental results, Golf (2018), and numerical results of the open water coefficients for 2000 RPM not taking into account uncertainties.

4.2 Cavitating flow

The inception diagram constructed using the experimental tests by Golf (2018) is shown in Figure 5. It indicates that the two simulated operating points 1 and 2 fall in regions where multiple cavitation topologies are present: hub vortex, tip vortex and sheet cavitation. Comparison between experimental

Table 2: Verification study using Eça and Hoekstra (2014) for the three different intervals of advance ratios J dictated by the different flow regimes: for $0.28 \leq J \leq 0.68$ flow separation is present, for $0.72 \leq J \leq 0.92$ separation is not visible anymore, and the interval $0.96 \leq J \leq 1.02$ is close to the zero-thrust condition.

J interval	$u_{num}(K_T)$	$u_{num}(10K_Q)$	$u_{num}(\eta_O)$
$0.28 \leq J \leq 0.68$	0.6%	1.4%	0.9%
$0.72 \leq J \leq 0.92$	1.0%	1.5%	0.5%
$0.96 \leq J \leq 1.02$	1.1%	2.9%	2.1%

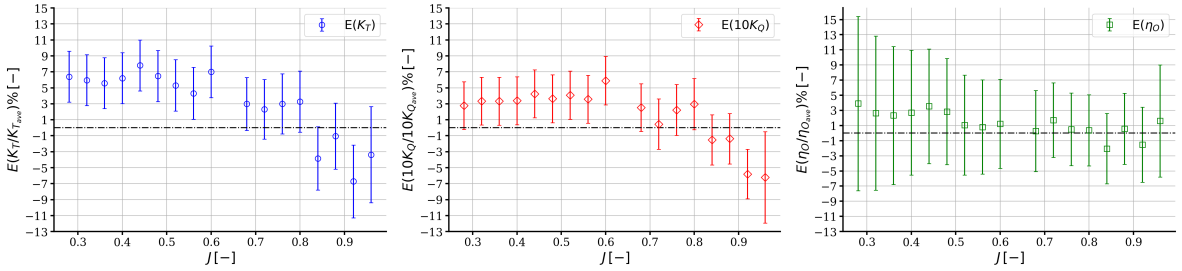

(a) Thrust coefficient K_T. (b) Torque coefficient $10K_Q$. (c) Open water efficiency η_O.

Fig. 4: Validation study following (ASME , 2009) procedure. Values of advance ratios J close to zero-thrust condition were omitted for clarity.

observations and numerical predictions of cavitation for these points shows that the area over which the cavity extends on the blade is comparable between the predictions and measurements (Figures 6 and 7). The inception of cavitation at the leading edge for Point 1 starts, for the experiments (Figure 6a), between 55 and 60 mm along the blade radius, while for the simulations (Figure 6b), onset of cavitation occurs between 50 mm and 55 mm along the radius; at the trailing edge, the cavity extends from circa 65 mm of the propeller radius to its tip in both cases. For Point 2 (Figures 7a and 7b), the inception at the leading edge is found between 50 mm and 55 mm of the propeller's radius for both experimental and numerical visualizations; at the trailing edge where the cavity extends from 70 mm of the radius to the tip of the blade in experimental photographs and simulations alike. In Figures 6 and 7 cavitation iso-surfaces were defined by a vapour volume fraction equal to 0.1. For both operating points, a slight under-prediction of the cavity volume and a steady-state is visible in the numerical solutions. Furthermore, the propagation of the cavity into tip vortex was not captured due to the use of RANS and the limited grid density (Lloyd et al. , 2017).

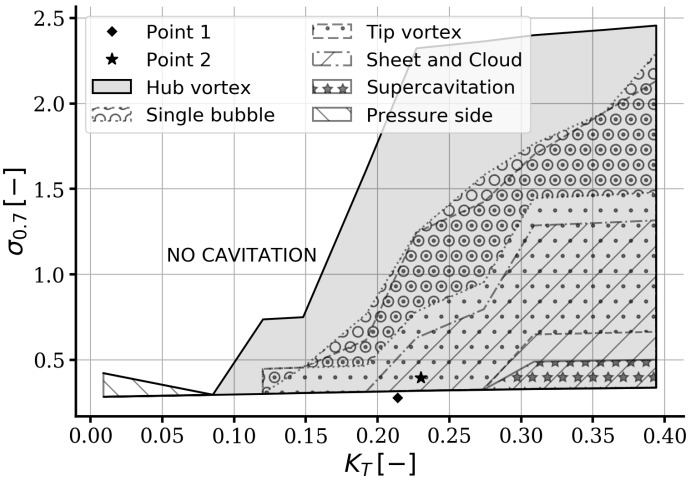

Figure 5: Representation of the cavitation inception diagram obtained via the experimental tests (Golf , 2018) and the location of the simulated operating points.

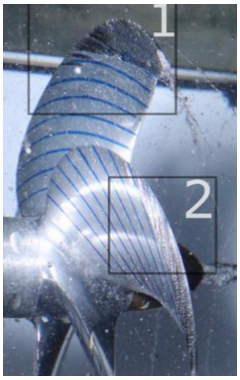

(a) Experiments

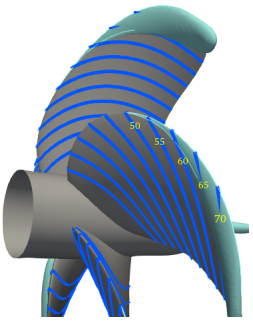

(b) Simulations

Fig. 6: Comparison of the cavitation pattern at operating Point 1.

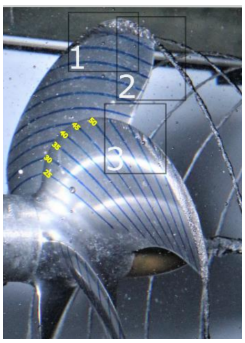

(a) Experiments

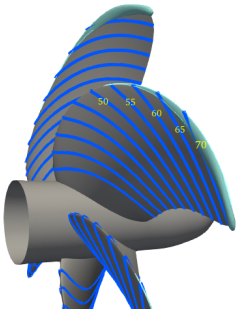

(b) Simulations

Fig. 7: Comparison of the cavitation pattern at operating Point 2.

5 Conclusions

The numerical study of the DPTC showed good agreement with the experimental work, both for wetted and cavitating conditions, with a maximum difference in wetted flow force coefficients of 8%, not considering experimental nor numerical uncertainties. This difference is caused by the transitional character of the flow due to low Reynolds numbers and systematic errors in the experiments. Comparable cavity extents for cavitating flow were also presented. To improve the quality of the results of both methodologies, the following suggestions can be taken into consideration: a more in depth analysis of the possible errors and uncertainties due to the measuring systems of the experimental setup due to the age of the apparatus; measurements of the inlet velocity during the cavitation tests to better define operating points tested (current velocity data were not reliable due to a malfunction of the measuring system while the tunnel was pressurized); application of transitional models (due to the limited dimensions of the propeller and intermediate Reynolds numbers), and investigation of different turbulence models to analyse the possibility to achieve higher quality results for the wetted flow; variation of time step to study the uncertainties of the temporal discretisation, local grid refinement should also be considered to better capture flow structures, such as tip vortex, important for the prediction of cavitating flow. Additionally, bubble, cloud and pressure side cavitation topology, as well as dynamic cavitation, could be explored by overcoming the limits imposed by the Volume of Fluid (VoF) methodology, known to have limitations in keeping a sharp interface, not offering detailed information on the cavity interface, nor allowing modeling of single bubbles.

Acknowledgements

The authors gratefully acknowledge the computing time granted by the Center for Computational Sciences and Simulation (CCSS) of the University of Duisburg-Essen and provided on the supercomputer magnitUDE (DFG grants INST 20876/209-1 FUGG, INST 20876/243-1 FUGG) at the Zentrum für Informations- und Mediendienste (ZIM). Additionally, the authors would like to acknowledge the Institute of Marine Technology, Maritime Engineering and Transport System (ISMT) for granting the use of the cavitation tunnel and Arjan Lampe from MARIN for generating the geometry of the propeller used for the numerical study.

References

R. Golf (2018). Kavitationsuntersuchung am DTC Propeller. B.Sc. Thesis, ISMT, University of Duisburg-Essen, Germany.

O. el Moctar, V. Shigunov, and T. Zorn (2012). Duisburg Test Case: Post-Panamax Container Ship for Benchmarking. *Sh Technol Res*, **59**(3), 50–64.

R. Dinter (2011). Fehlerrechnung für Einsteiger. Lecture notes TUHH.

F. R. Menter, Y. Egorov and D. Rusch (2006). Steady and unsteady flow modelling using the k-$\sqrt{k}$L model. Proceedings of the 5th International Symposium on Turbulence, Heat and Mass Transfer, Dubrovnik, Croatia.

D. R. Rijpkema, J. Baltazar and J. Falcão de Campos (2015). Viscous flow simulations of propellers in different Reynolds number regimes. Proceedings of the 4th International Symposium on Marine Propulsors, Austin, Texas, United States.

J. Sauer, and G.H. Schnerr (2001). Development of a new cavitation model based on bubble dynamics. *Zeitschrift für Angewandte Mathematik und Mechanik*, **81**(S3), 561–562.

G. Vaz, D. Hally, T. Huuva, N. Bulten, P. Muller, P. Becchi, J.L.R. Herrer, S. Whitworth, R. Macé and A. Korsström (2015). Cavitating flow calculations for the E779A propeller in open water and behind conditions: code comparison and solution validation. Proceedings of the 4th International Symposium on Marine Propulsors, Austin, Texas, United States.

L. Eça, and M. Hoekstra (2014). A procedure for the estimation of the numerical uncertainty of CFD calculations based on grid refinement studies. *J Comput Phys*, **262**, 104–130.

L. Eça, and M. Hoekstra (2009). Evaluation of numerical error estimation based on grid refinement studies with the method of the manufactured solutions. *Journal of Computers and Fluids*, **38**, 1580–1591.

ASME (2009). *Standard for Verification and Validation in Computational Fluid Dynamics and Heat Transfer: ASME V&V 20-2009.* American Society of Mechanical Engineers.

T. Lloyd, G. Vaz, D. Rijpkema and A. Reverberi (2017). Computational fluid dynamics prediction of marine propeller cavitation including solution verification. Proceedings of the 5th International Symposium on Marine Propulsors, Espoo, Finland.